Melt penetration in oceanic lithosphere: Li isotope records from the Pozantı-Karsantı ophiolite in southern Turkey

BEN-XUN SU [1, 2*], CHEN CHEN [1, 2], KWAN-NANG PANG [3], PATRICK ASAMOAH SAKYI [4], IBRAHIM UYSAL [5], ERDI AVCI [6], XIA LIU [1, 7], PENG-FEI ZHANG [8]

[1] Key Laboratory of Mineral Resources, Institute of Geology and Geophysics, Chinese Academy of Sciences, Beijing 100029, China

[2] University of Chinese Academy of Sciences, Beijing 100049, China

[3] Institute of Earth Sciences, Academia Sinica, Taipei, Taiwan

[4] Department of Earth Science, University of Ghana, P. O. Box LG 58, Legon-Accra, Ghana

[5] Department of Geological Engineering, Karadeniz Technical University, 61080-Trabzon, Turkey

[6] Department of Geological Engineering, İstanbul University, 34320, İstanbul, Turkey

[7] College of Earth Sciences, Chendu University of Technology, Chengdu 610059, China

[8] Department of Earth Sciences, the University of Hong Kong, Pokfulam Road, Hong Kong, China

* Corresponding Author

subenxun@mail.igcas.ac.cn

ABSTRACT

Understanding melt penetration in ophiolites is important in revealing the formation and evolution of the oceanic lithosphere, as well as the formation of chromite deposits. We conducted *in situ* Li isotope analysis of olivine grains from the harzburgite, podiform chromitite and dunite envelope of the mantle sequence, and dunite and wehrlite cumulates from the crustal sequence of the Pozantı-Karsantı ophiolite. Olivine in the different rocks has variable and distinctive Li concentrations (0.95 to 2.01 ppm) and δ^7Li

isotopic compositions (-5.43 to 16.65 ‰). The olivine in the refractory harzburgite of the Pozantı-Karsantı ophiolite extends from MOR-peridotite-like compositions to lower δ^7Li values and higher Li concentrations, suggesting ingressive Li diffusion via melt penetration. The Li isotopic compositions of the olivine in the dunite envelope and podiform chromitite represent the compositions of their parental melts and thus their sources. The dunite envelope has δ^7Li values beyond MORB and OIB variations and overlaps the arc lava range, suggesting an affinity with arc magmatism. The podiform chromitite, on the other hand, shows wider δ^7Li variation and overall lower values, falling in the ranges of granulite and eclogite. The parental melts of the podiform chromitite might: (1) originate from partial melting of a dehydrated and metamorphosed subducted slab or (2) may initially have had the same isotopic composition as the associated dunite, but later experienced compositional modification by fluids. The Li isotopic compositions of the dunite and wehrlite cumulates fall between the OIB and arc fields, supporting a subduction origin for these ultramafic cumulates and their arc-like parental magmas. The Pozantı-Karsantı ophiolite records various melt penetration agents during its formation and evolution. The melts display progressive compositional variations, mainly between OIB and immature and mature oceanic island arc magmatism, pointing to their correlation with subduction initiation. The distinctive Li isotopic compositions of the Pozantı-Karsantı, Luobusa and Trinity ophiolites suggest that the generation and compositions of penetrating melts in oceanic lithosphere and subsequent formation of chromite deposits are strongly controlled by tectonic setting. Consequently, Li isotope systematics can be used as an indicator of the tectonic setting and mineralization of ophiolites.

KEY WORDS: *Chromite; Li isotopes; melt penetration; olivine; ophiolite; subduction*

INTRODUCTION

Ophiolites are remnants of ancient oceanic lithosphere and commonly preserve imprints of mantle-derived melt invasion and differentiation (e.g., Pearce *et al*., 1984; Aitchison *et al*., 2000). The melt imprints occur in a variety of forms, such as lavas and intrusions in the crust and ultramafic veins and lenses in the mantle sequence of ophiolites (e.g., Dilek & Furnes, 2009, 2011). They are directly linked to the generation and evolution of the oceanic lithosphere as well as to the formation of chromite deposits (Ballhaus, 1998; Rollinson, 2008; Arai & Miura, 2016). In general, supra-subduction zone (SSZ) ophiolites are known to have experienced significant melt penetration relative to mid-ocean ridge (MOR) ophiolites, resulting in the formation of high-Cr chromite deposits compared to high-Al chromite deposits in the latter (Pearce *et al*., 1984; Arai & Yurimoto, 1994; Zhou *et al*., 1994, 1998). The occurrence of chromite deposits is also different at different structural levels within ophiolites, namely; podiform deposits occur in the mantle peridotites, whereas stratiform deposits occur in crustal cumulate zones (Paktunc, 1990; Saka *et al*., 2014; Arai & Miura, 2016). Therefore, the identification of the nature and origin of the melts penetrating a given ophiolite is critical in addressing the tectonic setting in which the ophiolite formed, as well as the type and scale of associated mineralization. However, the genetic relationship between melt penetration occurring at different levels of ophiolites is usually not fully constrained, partly due to isotopic data not being obtained from rocks in the mantle sequence.

Olivine is the major constituent mineral in both mantle rocks and crustal cumulates. It is the dominant mineral phase of dunite that envelopes a podiform chromite body or is interlayered with stratiform chromitite (Paktunc *et al*., 1990; Arai & Miura, 2016). Given that the mineral assemblage in chromitites consists only of olivine + chromite in varying modal proportions, and that chromite structurally contains minor or no Li, the Li contents and isotopic compositions in olivine in chromitites are representative of the whole-rock samples (Su *et al*., 2016). Olivine can preserve primary Li elemental and isotopic compositions which may be used to trace high-temperature processes (Su *et al*., 2014; Tang *et al*., 2014). This is due to the conspicuously slower diffusion rate of Li in olivine than in pyroxene (Dohmen *et al*., 2010) and the immunity of Li in olivine to sub-solidus Fe-Mg exchange between olivine and chromite (Bai *et al*., 2017; Su *et al*., 2017). Lithium behaves as a moderately incompatible element during high-temperature magmatic processes (Brenan *et al*., 1998; Woodland *et al*., 2004); however, no significant Li isotope fractionation is believed to occur during partial melting and fractional crystallization (Tomascak *et al*., 1999; Bryant *et al*., 2004; Teng *et al*., 2006; Magna *et al*., 2010). Lithium isotope systematics have, thus, been used to constrain the nature and origin of magmatism (e.g., Elliott *et al*., 2006; Chan *et al*., 2002) and melt infiltration (Decitre *et al*., 2002; Lundstrom *et al*., 2005; Gao *et al*., 2011; Su *et al*., 2016) that have contributed to the evolution of the oceanic lithosphere.

This study presents *in situ* Li isotopic data for olivine from ultramafic rocks and associated chromitites from the Pozantı-Karsantı ophiolite in southern Turkey. We examine the behavior of Li and its isotopes during serpentinization, and subsequently attempt to constrain the nature, origin and genetic relationships among the parental melts

responsible for the formation of podiform chromitites, the dunite envelope and crustal cumulates.

GEOLOGY OF THE POZANTI-KARSANTI OPHIOLITE AND SAMPLE COLLECTION

The Pozantı-Karsantı ophiolite, exposed in the eastern Tauride belt, is located 60 km north of the city of Adana in southern Turkey (Fig. 1a). It covers an area of approximately 1300 km^2, with a length of 100 km and width of 30 km (Fig. 1b). The ophiolite is associated with an ophiolitic mélange and its metamorphic sole rests in tectonic contact with underlying platform carbonates of Late Devonian to Early Cretaceous age (Fig. 1c; Tekeli *et al*., 1983; Dilek & Moores, 1990; Robertson, 2002). The ophiolite sequence consists mainly of tectonized peridotites, mafic-ultramafic cumulates and isotropic gabbros (Fig. 1c). The ultramafic cumulates occur as a large massif of dunite and wehrlite (Figs 1b, 2a), with minor layers of dunite and clinopyroxenite (Fig. 2b). The occurrence of rhythmic layers of chromitite and dunite in the ultramafic cumulates (Fig. 2c) is inferred to be close to the petrological Moho (Fig. 1c; Parlak *et al*., 2000, 2002). The chromitite in the mantle harzburgite typically has a podiform structure (Fig. 2d) and is variable in morphology, from massive and disseminated to nodular and banded. Previous studies have suggested that the chromitite is of the high-Cr variety formed from boninitic melts (Avc *et al*., 2017).

Swarms of gabbro and diabase dykes cut the Pozantı-Karsantı ophiolitic units at different structural levels, as well as the metamorphic sole (Lytwyn & Casey, 1995; Dilek *et al*., 1999; Parlak, 2000; Lian *et al*., 2017a). Geochronological studies indicate ages of 107-83 Ma for the metamorphic sole (Thuizat *et al*., 1981; Dilek *et al*., 1999; Çelik, 2008) and 92-87 Ma for the mafic dykes and mafic cumulates (Dilek *et al*., 1999; Lian *et al*., 2017a). These results suggest that the ophiolite formed during the Late Cretaceous, presumably in the Neotethys Ocean (Dilek & Moores, 1990; Polat *et al*., 1996; Robertson, 2002; Dilek & Furnes, 2009). The metamorphic sole, mafic cumulates and dyke swarm all display transitional geochemical compositions between MORB and typical island arc lavas (Lytwyn & Casey, 1995; Parlak *et al.,* 2002; Çelik, 2007; Lian *et al*., 2017a). This has led to ongoing debates about the tectonic setting of the Pozantı-Karsantı ophiolite. Based on its SSZ nature, some authors have proposed that the ophiolite resulted from immature island arc magmatism during subduction initiation (e.g., Pearce *at al*., 1984; Parlak *et al*., 2002; Dilek & Furnes, 2009), whereas others suggested that it formed along a mid-ocean ridge north of the Tauride Platform and constituted part of the forearc mantle wedge (e.g., Lytwyn & Casey, 1995; Polat *et al*., 1996; Saka *et al*., 2014).

In this study, 75 samples were collected from different units of the Pozantı-Karsantı ophiolite. After screening, 15 least-altered samples were selected for mineral separation and chemical analysis. The sample set includes three harzburgites, three dunites and five chromitite samples from the mantle sequence, and three dunite and one wehrlite samples from the ultramafic cumulate unit. No fresh olivine was found in the chromitite samples from the stratiform layers. The geographic locations and structural levels of these samples are given in Table 1.

ANALYTICAL METHODS

Li isotope analysis

Olivine grains were handpicked under a binocular microscope, and together with olivine standard 06JY31OL were mounted in an epoxy mount. The mount was then polished to expose the crystals as shown in Fig. 3. Pre-analytical transmitted and reflected light images of all the olivine grains were obtained for correct identification of the analyzed grains. To reveal the spatial variations in Li concentrations and Li isotopic compositions, a thin section was used for sample PK14-41. The samples were vacuum-coated with high-purity gold and analyzed using Cameca IMS 1280HR SIMS at the Institute of Geology and Geophysics, Chinese Academy of Sciences (IGGCAS). The O^- primary ion beam was accelerated at 13 kV, with an intensity of about 15 to 30 nA. The elliptical spot was approximately 20 × 30 μm in size. Positive secondary ions were measured on an ion multiplier in pulse counting mode, with a mass resolution (M/DM) of 1500 and an energy slit open at 40 eV without any energy offset. A 60-second pre-sputtering with raster was applied before analysis. The secondary ion beam position in apertures, as well as the magnetic field and the energy offset, were automatically centred before each measurement. Eighty cycles were measured with counting times of 7 and 2 seconds for ^6Li and ^7Li, respectively. The measured δ^7Li values are given as δ^7Li ($[(^7Li/^6Li)_{sample}/(^7Li/^6Li)_{L\text{-}SVEC}-1] \times 1000$) relative to units of the standard NIST SRM 8545 (L-SVEC) with $^7Li/^6Li$ of 12.0192. The instrumental mass fractionation is

expressed in $\Delta i = \delta^7Li_{SIMS} - \delta^7Li_{MC\text{-}ICPMS}$. The olivine standard 06JY31OL with an Mg# of 91.2, Li concentration of 2.70 ± 0.60 ppm and δ^7Li of 4.51 ± 0.33‰ (Su *et al*., 2015) was used as a standard; twenty one analyses of the standard in this study yielded a homogeneous Li isotopic composition with an instrumental mass fractionation of Δi = 1.82 ± 0.30‰ (1SD). Lithium concentration of the samples was calculated on the basis of $^7Li^+$ count rates (cps/nA) relative to the standard. The detection limit of Li concentration measurements is <1 ppb and uncertainty is mostly <0.90 ppm (1σ). The internal errors of the Li isotopic compositions for both the standard and the olivine samples are less than 1.20‰ (1se), while internal errors for serpentine are less than 2.20‰. Matrix effects, in which δ^7Li increases by 1.0‰ for each mole percent decrease in the Fo content of olivine (Su *et al*., 2015), were considered for calibration.

Major element analysis

Major element compositions of minerals were determined by wavelength dispersive spectrometry using JEOL JXA8100 electron probe microanalyzer (EPMA) at the IGGCAS. Analytical spots were located close to the previous SIMS analytical spots, and the analysis was conducted at the operating conditions of 5 μm beam diameter, 10 nA beam current, 15 kV accelerating voltage and 10-30 s counting time on peak. Natural (jadeite [$NaAlSiO_6$] for Na, Al and Si, rhodonite [$MnSiO_3$] for Mn, sanidine [$KAlSi_3O_8$] for K, garnet [$Fe_3Al_2Si_3O_{12}$] for Fe, Crdiopside [$(Mg, Cr)CaSi_2O_6$] for Ca, olivine [$(Mg, Fe)_2SiO_4$] for Mg) and synthetic (rutile for Ti, 99.7% Cr_2O_3 for Cr, Ni_2Si for Ni) minerals

were used for standard calibration, and a program based on the ZAF procedure was used for matrix corrections. Detection limits of of the major elements are <180 ppm, and analytical uncertainty is better than 1.5% (1SD).

RESULTS

The Li concentration, δ^7Li and major oxide compositions of olivine in the studied samples from the Pozantı-Karsantı ophiolite are reported in Table 2. In general, the olivine has a Fo content of 88.7-94.9, NiO of 0.11-0.51 wt % and MnO of 0.05-0.20 wt %, all of which fall within the ranges of previously published data (Parlak *et al*., 2002; Saka *et al*., 2014; Avc *et al*., 2017; Lian et al., 2017b). The Fo contents are well correlated with both NiO and MnO contents (Fig. 4a, b), following the general trends of partial melting and fractional crystallization. Relative to the olivine from the crustal cumulates, the rocks of the mantle sequence display large Fe/Mn variations in olivine at a given Fo (Fig. 4c).

The studied olivine grains have Li concentrations varying from 0.95 to 2.01 ppm, a range comparable with that of mantle olivines (1.0-1.8 ppm; Seitz *et al*., 2004; Woodland *et al*., 2004; Su *et al*., 2014). The analyses yielded δ^7Li values ranging from -5.43 to 16.65 ‰. Both the Li concentrations and the δ^7Li values of olivine in the chromitite and the enveloping dunite exhibit roughly negative correlations with Fo and NiO, and positive correlations with MnO (Fig. 5). The olivines in the dunite and wehrlite cumulates have restricted Li contents of 1.2-1.7 ppm and plot away from the correlation trends defined by those in the rocks of the mantle sequence (Fig. 5a-c), while their δ^7Li values are relatively homogeneous and generally higher than those in the mantle

sequence (Fig. 5d-f). The serpentine in nodular chromitite sample PK14-41 has extremely low Li concentrations of 0.09-0.24 ppm and low δ^7Li values of -23.14 to -8.73 ‰ (Table 2).

DISCUSSION

Behavior of Li isotopes during serpentinization

Lithium is a fluid-mobile element, implying that its concentration and isotopic composition in rocks and minerals may vary during alteration. It has been documented that variations in the Li concentration and Li isotope composition of altered basaltic and peridotitic rocks depends on the nature of the fluid and temperature (Chan *et al*., 1992, 2002; Decitre *et al*., 2002; Lundstrom *et al*., 2005; Vils *et al*., 2008, 2009). Seawater-basalt exchange at low temperatures could result in Li enrichment and a δ^7Li increase in altered basalts, compared to fresh basalts, due to the uptake of seawater Li into the alteration products (e.g., smectites) (Chan *et al*., 1992, 2002), whereas hydrothermally altered rocks may become depleted in Li concentration and isotopically light as a result of high-temperature hydrothermal extraction at crustal levels and preferential partitioning of ^{6}Li into greenschist and amphibolite facies minerals and serpentine (Chan *et al*., 2002; Vils *et al*., 2008, 2009). During serpentinization of oceanic peridotites, “relict” minerals (olivine and pyroxenes) generally have lower Li concentrations and higher δ^7Li values, while the reverse is observed in serpentine and chlorite (Decitre *et al*., 2002). Decitre *et al*. (2002), therefore, inferred that the Li content

of the initial hydrothermal fluid was dominated by oceanic basalt-derived Li, which easily overwhelmed the very low Li content originally present in seawater. Accordingly, the authors proposed that serpentine incorporated Li and preferentially ^{6}Li from the hydrothermal fluid. A similar negative correlation between Li and δ^{7}Li in olivine was observed in a serpentinized peridotite sample from the Trinity ophiolite, but this was interpreted as the result of preferential leaching of ^{6}Li from the mineral grains during serpentinization (Lundstrom *et al*., 2005).

The Li depletion and low δ^{7}Li values of the serpentine in the studied chromitite (Table 2) cannot be ascribed to low-temperature seawater-rock exchange, whereas the negative correlation (Fig. 6) also rules out high-temperature hydrothermal extraction at near surface levels. Although the low δ^{7}Li signature and its negative correlation with Li concentration in the serpentine is consistent with the observations by Decitre *et al*. (2002), the confirmed preferential partitioning of ^{6}Li in serpentine relative to fluid, and the Li depletion (0.09-0.24 ppm) (Fig. 6) apparently differ from that of the serpentine (several to tens of ppm) reported in Decitre *et al*. (2002). These discrepancies imply that the serpentinizing fluids may have distinct compositions, possibly poor in Li and enriched in ^{6}Li. Such fluids might be related to melting of a dehydrated subducted slab (Zack *et al*., 2003; Nishio *et al*., 2004; Su *et al*., 2012, 2016; Tang *et al*., 2012, 2014), but whether an isotopically light domain in the mantle could be produced via slab subduction and dehydration is still contentious (Benton *et al*., 2004; Marschall *et al*., 2007; Penniston-Dorland *et al*., 2012).

Alternatively, the serpentinizing fluid could have been derived from the surface of chromite crystals (Matveev & Ballhaus, 2002). It has been experimentally documented that in immiscible basalt-water systems chromite and olivine can be physically

fractionated due to the differential wetting properties of fluid and melt against oxide and silicate surfaces; chromite collects the exsolved fluid, whereas olivine remains in the melt (Ballhaus, 1998; Matveev & Ballhaus, 2002). Our field survey revealed that intense serpentinization selectively occurs in the podiform chromitite body relative to the enveloping dunite and harzburgite host. At a microscopic scale, the degree of serpentinization decreases away from chromite bands (Su *et al*., 2016) or nodules (Fig. 6a). Also, there is a correlation between the Li concentration and δ^7Li of the serpentine away from chromite nodules (Fig. 6b). These features support the derivation of fluids from the chromite surface. The spatial variations in the compositions of the serpentine might reflect mixing of Li isotopes between relict olivine and serpentinizing fluids, and further indicate the extreme depletion of Li in the initial fluids, thereby confirming the preferential leaching of ^{6}Li from olivine grains during serpentinization (Lundstrom *et al*., 2005). This implies that the surface fluids associated with chromite (Ballhaus, 1998; Matveev & Ballhaus, 2002) differ from common hydrothermal fluids that evolve from magmas (Li-poor vs. Li-rich).

Fe-Mg exchange and Li diffusion effects on the mantle sequence of the ophiolite

Fe-Mg exchange

Sub-solidus Fe-Mg inter-diffusion between olivine and chromite has been well documented in studies of layered intrusions and ophiolites, during which there is an exchange between Mg in chromite and Fe in olivine (Jackson, 1969; Melcher *et al*., 1997; Xiao *et al*., 2016; Bai *et al*., 2017). This process would lead to relatively large variations of Fo and Fe/Mn ratio and limited NiO and MnO variations in the olivine as observed in

the dunite envelope and chromitite of the Pozantı-Karsantı ophiolite (Fig. 4). Nonetheless, the Li isotope systematics of the olivine would not be affected by Fe-Mg exchange with chromite because of the null Li content in chromite (Su *et al*., 2016). The olivines in the dunite and wehrlite cumulates exhibit homogeneous Fo and Fe/Mn ratios (Fig. 4), indicating a negligible effect of Fe-Mg exchange between olivine and chromite or clinopyroxene. As a consequence, the homogeneous Li element and isotopic compositions in olivine individual grains (Table 2) should represent their initial compositions after crystallization.

Li diffusion

Lithium diffusion may occur at intra- and inter-grain scales, and between melts and minerals, generally inducing relatively heterogeneous compositions in individual mineral grains in the former case (Seitz *et al*., 2004; Rudnick & Ionov, 2007; Richter *et al*., 2014; Tomascak *et al*., 2016). Core-rim profile analyses on the olivine grains from all rock types in this study reveal homogeneous Li concentrations within analytical uncertainty and mostly <2‰ δ^7Li difference in individual grains (Table 2), ruling out the possibility of intra-grain diffusion. Similarly, inter-grain diffusion would not account for the above-mentioned olivine compositions of the dunite and chromitite, since the associated chromite contains little or no Li.

The olivine grains in the Pozantı-Karsantı harzburgites exhibit slightly higher Li concentrations than those in MOR-peridotites (Fig. 7), reflecting Li diffusive ingress after partial melting of the harzburgite. Their compositional variation also follows the Li diffusion trend defined by a harzburgite-dunite sample transect from the Trinity ophiolite

(Lundstrom *et al*., 2015). Generally, the Li concentrations and δ^7Li values of olivine in the Pozantı-Karsantı harzburgites are equal to or slightly higher than those in the dunite envelope and chromitites (Fig. 7). This is contrary to the theoretical prediction that a mineral phase can potentially receive Li via diffusion, only if it has relatively low Li, eventually resulting in low δ^7Li in the mineral (Jeffcoate *et al*., 2007; Magna *et al*., 2008; Dohmen *et al*., 2010; Richter *et al*., 2014). Thus, it is most likely that the harzburgite experienced percolation of the parental melts from which the dunite and chromitite had formed because mantle-derived melts generally have higher Li concentrations than residual harzburgites (e.g., Tomascak *et al*., 2008; Xiao et al., 2017). The overall low and variable Li signatures of the olivine in the dunite envelope and chromitite (Fig. 5a-c) probably resulted from fractional crystallization as olivine is the earliest crystallizing phase and Li is a moderately incompatible element that prefers to stay in the melt during magma differentiation (Brenan *et al*., 1998; Tomascak *et al*., 1999; Chan & Frey, 2003; Teng *et al*., 2006; Su *et al*., 2017). Therefore, the olivine in the dunite envelope and chromitite, as well as the dunite and wehrlite cumulates, preserves the primary Li and δ^7Li signatures from when they were formed. Taking into account that there is no Li isotope fractionation during partial melting and fractional crystallization (e.g., Tomascak *et al*., 1999; Teng *et al*., 2006), the Li isotopic compositions of these olivine grains should represent the compositions of their parental magmas and their sources.

Melt penetration in the Pozantı-Karsantı ophiolite

Melt penetration in the mantle harzburgite

The harzburgite from the Pozantı-Karsantı ophiolite preserves refractory chemical compositions (e.g., high Mg# and Cr#) in minerals (Fig. 4; Saka *et al*., 2014; Lian *et al*., 2017b) and depletions in whole-rock Al_2O_3, CaO and rare earth element (REE) contents (Saka *et al*., 2014). It has, therefore, been suggested that the harzburgite was residual after partial melting in a MOR environment (Saka *et al*., 2014). This inference could be argued based on the major element and Li isotopic compositions of the major minerals. Low Al_2O_3 and TiO_2 in pyroxene and chromite in the harzburgite are more comparable with those in SSZ-type peridotites (Saka *et al*., 2014; Lian *et al*., 2017b). The δ^7Li values of the olivine in the Pozantı-Karsantı harzburgite only partially overlap the range of those in the Gakkel Ridge peridotites, but the former mostly extend to lower values (Fig. 7). Furthermore, the harzburgite is also characterized by slight to moderate whole-rock enrichments in light REE and large ion lithophile elements, reflecting variable metasomatism (Saka *et al*., 2014). These results suggest that the Pozantı-Karsantı harzburgite more likely formed in a SSZ setting and suffered a high degree of melt extraction and subsequent melt percolation. The similar Li isotopic composition to the Luobusa harzburgite (Fig. 7) implies that the metasomatic melts might be arc-like lavas with low δ^7Li values (Su *et al*., 2016).

Parental melts of the dunite envelope and podiform chromitite

It is widely accepted that the podiform chromitite and dunite envelopes of ophiolites are of magmatic origin and normally show variable compositions, depending on the nature of the parental melts and tectonic setting (Arai & Miura, 2016 and references therein). The dunite and chromitite in the mantle sequence of the Pozantı-Karsantı ophiolite exhibit

larger variations in the major element compositions of their constituent minerals than other rock units in the same ophiolite (Fig. 4; Saka *et al*., 2014; Avc *et al*., 2017), and these major element variations are not well correlated with Li concentration and δ^7Li (Fig. 5). These features indicate that the dunite-chromitite association, despite its similar occurrence (Fig. 2d), did not form from a single parental melt but was different from pod to pod. Nonetheless, the compositional variation of their parental melts might be continuous, as reflected in the good correlation between Li and δ^7Li in the dunite envelopes (Fig. 7). The δ^7Li values of the dunite envelopes extend beyond MORB and OIB (ocean island basalt) variations and overlap the arc lava range (Fig. 7), suggesting their affinity with arc magmatism.

Relative to the dunites, the podiform chromitites show wider δ^7Li variations and overall lower values, and roughly negative correlation between Li and δ^7Li (Fig. 7). These differences can be ascribed to two possibilities: (1) The decrease in δ^7Li from dunite to chromitite is comparable to that in the Luobusa ophiolite, which is in the range of granulites and eclogites (Fig. 7; Su *et al*., 2016). It was previously interpreted that the parental melts of the podiform chromitite might have originated from the melting of a dehydrated and metamorphosed subducted slab. Such melts, together with the abovementioned arc-like melts, continuously and progressively reacted with the oceanic lithospheric mantle, resulting in the formation of the dunite and chromitite, and accounting for the observed Li isotope heterogeneity; (2) The podiform chromitite and associated dunite were generated from a common arc-like melt and initially had the same isotopic compositions. Subsequently, the olivine in the podiform chromitite was compositionally (Li isotopes at least) modified by surface fluids from the chromite as discussed above. As the amount of surface fluids depends on the size and quantity of

chromite grains, the occurrence of more chromite grains in chromitite will favor the release of more fluid, which will result in significant modification of the olivine composition. This can explain the larger δ^7Li variations in the banded and massive chromitite samples than in the disseminated ones (Fig. 5).

Magmatism events at crustal level and implications for initial subduction

Previous studies have revealed that the ultramafic cumulates of the Pozantı-Karsantı ophiolite are compositionally distinct from those in MOR and back-arc basin ophiolites, and represent part of the plutonic core of an intra-oceanic island arc (Parlak *et al*., 2002; Saka *et al*., 2014) or that formed in a fore-arc tectonic setting (Polat *et al*., 1996). The Li isotopic compositions of the ultramafic cumulates plot away from MORB and fall between OIB and arc lava fields (Fig. 7), further supporting the subduction origin of these ultramafic cumulates and their arc-like parental magmas. Furthermore, the overlapping and restricted δ^7Li ranges of the cumulate dunites and wehrlites (Fig. 7) suggest their derivation from a common parental magma. In addition, the absence of plagioclase and enrichment of clinopyroxene in the ultramafic cumulates (Dilek & Furnes, 2009; Parlak *et al*., 2009; Saka *et al*., 2014) indicate that the parental magmas are hydrous in nature (Niu, 2005) and are likely related to dehydration of a subduction slab.

From ultramafic to mafic cumulates, progressive changes in the geochemical compositions in terms of both major and trace element concentrations (Polat *et al*., 1996; Saka *et al*., 2014) indicate their genetic relationships. This was controversially interpreted as compositional changes in their source, from felsic upper crust to mafic-dominant immature oceanic island arc crust (Polat *et al*., 1996) and also attributed to variable

degrees of fractional crystallization of a parental melt (Saka *et al*., 2014). The consensus is that the parental melts of the ultramafic and mafic cumulates were derived from typical arc magmatism. In contrast, rocks of the earlier metamorphic sole show a progressive compositional variation from N- to E-MORB, through OIB to island arc tholeiites (IAT) (Polat *et al*., 1996; Çelik, 2007), while the latest mafic dykes intruding the Pozantı-Karsantı ophiolite and metamorphic sole are compositionally similar to island arc lavas and are thought to have been produced during intra-oceanic subduction (Lytwyn & Casey, 1995; Polat *et al*., 1996; Lian *et al*., 2017a).

In summary, the Pozantı-Karsantı ophiolite records the penetration of various melts during its formation and evolution. These melts display progressive compositional variations mainly between OIB and immature and mature oceanic island arc magmatism, pointing to their correlation with initial subduction. During the initial stage of subduction, diverse materials including marine sediments, altered and fresh oceanic crust were probably incorporated into the melt or were part of the package of rocks that underwent partial melting (Fig. 8). These materials had highly variable in Li isotope compositions (Tang *et al*., 2007; Tomascak *et al*., 2016) which could account for the large Li isotopic variations in the Pozantı-Karsantı ophiolite. In comparison, the Luobusa ophiolite hosting an economic chromite deposit was believed to have formed in a mature island arc (Zhou *et al*., 1996; Su *et al*., 2016), whereas the chromite-barren Trinity ophiolite formed in a back-arc basin (Lundstrom *et al*., 2015). The distinct Li isotopic compositions among these three ophiolites (Fig. 7) suggest that the generation and compositions of penetrating melts in the oceanic lithosphere and subsequent formation of the chromite deposits were strongly controlled by tectonic setting.

CONCLUSIONS

The olivine of the Pozantı-Karsantı ophiolite has variable Li concentrations (0.95 to 2.01 ppm) and δ^7Li values (-5.43 to 16.65 ‰). The refractory harzburgite preserves only partly MOR-peridotite-like Li isotopic compositions and mostly extends to lower δ^7Li values and higher Li concentrations, suggesting a high degree of initial melt extraction and subsequent arc-like melt penetration processes. The δ^7Li values of the dunite envelope reveal the affinity of their parental magmas to arc magmatism, while the parental melts of the podiform chromitites: (1) might have originated from melting of a dehydrated and metamorphosed subducted slab, or (2) were the same as the associated dunite but later suffered compositional modification by surface fluids associated with chromites. The Li isotopic compositions of the dunite and wehrlite cumulates fall between OIB and arc lava fields, supporting the subduction origin of these ultramafic cumulates and their arc-like parental magmas. These results, together with previous studies of the metamorphic sole rocks and mafic cumulates and dykes, indicate that the Pozantı-Karsantı ophiolite formed in a SSZ environment during initial subduction and experienced percolation by various melts. Comparisons with data for the Luobusa and Trinity ophiolites suggest that tectonic setting controls the generation and compositions of penetrating melts in the oceanic lithosphere and the subsequent formation of chromite deposits.

ACKNOWLEDGEMENTS

We would like to thank Di Zhang, Guo-Qiang Tang and Yu Liu for their assistance with the electron microprobe and SIMS analyses. Very constructive and detailed comments from Simon Turner, Paul Tomascak, Joyashish Thakurta and an anonymous reviewer are greatly appreciated.

FUNDING

This study was supported by the National Natural Science Foundation of China (Grant 41772055) and the State Key Laboratory of Lithospheric Evolution (Grant 201701).

REFERENCES

Aitchison, J.C., Davis, A.M., Liu, J., Luo, H., Malpas, J.G., McDermid, I.R.C., Wu, H., Ziabrev, S.V.,Zhou, M.F., 2000. Remnants of a Cretaceous intra-oceanic subduction system within the Yarlung–Zangbo suture (southern Tibet). Earth and Planetary Science Letters 183, 231-244.

Arai, S., Miura, M., 2016. Formation and modification of chromitites in the mantle. Lithos 264, 277-295.

Avcı, E., Uysal, İ., Akmaz, R. M., Saka, S., 2017. Ophiolitic chromitites from the Kızılyüksek area of the Pozantı-Karsantı ophiolite (Adana, southern Turkey): Implication for crystallization from a fractionated boninitic melt. Ore Geology Reviews doi.org/10.1016/j.oregeorev.2016.08.033.

Bai, Y., Su, B.X., Chen, C., Yang, S.H., Liang, Z., Xiao, Y., Qin, K.Z., Malaviarachchi, S.P.K., 2017. Base metal mineral segregation and Fe-Mg exchange inducing extreme compositions of olivine and chromite from the Xiadong Alaskan-type complex in the southern part of the Central Asian Orogenic Belt. Ore Geology Reviews doi:10.1016/j.oregeorev.2017.01.023.

Ballhaus, C., 1998. Origin of podiform chromite deposits by magma mingling. Earth and Planetary Science Letters 156, 185-193.

Brenan, J.M., Neroda, E., Lundstrom, C.C., Shaw, H.F., Ryerson, F.J., Phinney, D.L., 1998. Behaviour of boron, beryllium, and lithium during melting and crystallization: constraints from mineral-melt partitioning experiments. Geochimica et Cosmochimica Acta 62, 2129-2141.

Çelik, O.F., 2007. Metamorphic sole rocks and their mafic dykes in the eastern Tauride belt ophiolites (southern Turkey): implications for OIB-type magma generation following slab break-off. Geological Magazine 144, 849-866.

Çelik, O.F., 2008. Comparison of the K-Ar and ^{40}Ar-^{39}Ar dating methods: Examples from the metamorphic sole rocks of the southern Turkish ophiolites. Yerbilimleri 29, 101-110.

Chan, L.H., Edmond, J.M., Thompson, G., Gillis, K., 1992. Lithium isotopic composition of submarine basalts: implications for the lithium cycle in the oceans. Earth and Planetary Science Letters 108, 151-160.

Chan, L.H., Alt, J.C., Teagle, D.A.H., 2002. Lithium and lithium isotope profiles through the upper oceanic crust: a study of seawater–basalt exchange at ODP sites 504B and 896A. Earth and Planetary Science Letters 201, 187-201.

Decitre, S.E., Deloule, E., Reisberg, L., James, R., Agrinier, P., Mevel, C., 2002. Behavior of Li and its isotopes during serpentinization of oceanic peridotites. Geochemistry Geophysics Geosystem 3, 10.1029/2001GC000178.

Dilek, Y., Furnes, H., 2009. Structure and geochemistry of Tethyan ophiolites and their petrogenesis in subduction rollback systems. Lithos 113, 1-20.

Dilek, Y., Furnes, H., 2011. Ophiolite genesis and global tectonics: Geochemical and tectonic fingerprinting of ancient oceanic lithosphere. Geological Society of America Bulletin 123, 387-411.

Dilek, Y., Thy, P., Hacker, B., Grundvig, S., 1999. Structure and petrology of Tauride ophiolites and mafic dike intrusions (Turkey): Implications for the Neotethyan ocean. Geological Society of America Bulletin 111, 1192-1216.

Dohmen, R., Kasemann, S.A., Coogan, L., Chakraborty, S., 2010. Diffusion of Li in olivine. Part I: experimental observations and a multi species diffusion model. Geochimica et Cosmochimica Acta 74, 274-292.

Gao, Y.J., Snow, J.E., Casey, J.F., Yu, J.B., 2011. Cooling-induced fractionation of mantle Li isotopes from the ultraslow-spreading Gakkle Ridge. Earth and Planetary Science Letters 301, 231-240.

GDMRE (General Directrorate of Mineral Research and Exploration), 2002. 1:500.000 scaled Geological Maps of Turkey (Adana map section), Ankara-Turkey.

Jackson, E.D., 1969. Chemical variation in coexisting chromite and olivine in chromitite zones of the Stillwater Complex. Economic Geology Monograph 4, 41-71.

Jeffcoate, A.B., Elliott, T., Kasemann, S.A., Ionov, D., Cooper, K., Brooker, R., 2007. Li isotope fractionation in peridotites and mafic melts. Geochimica et Cosmochimica Acta 71, 202-218.

Lian, D., Yang, J., Dilek, Y., Liu, F., Wu, W., Xiong, F., 2017a. Geochemical, geochronological, and Sr-Nd isotopic constraints on the origin of the mafic dikes from the Pozanti-Karsanti ophiolite: Implications for tectonic evolution. The Journal of Geology 125, 223-239.

Lian, D., Yang, J., Dilek, Y., Wu, W., Zhang, Z., Xiong, F., Liu, F., Zhou, W., 2017b. Diamond, moissanite and other unusual minerals in podiform chromitites from the Pozanti-Karsanti ophiolite, southern Turkey: implications for the deep mantle origin and ultra-reducing conditions in podiform chromitite. American Mineralogist doi.org/10.2138/am-2017-5850.

Lundstrom, C.C., Chaussidon, M., Hsui, A.T., Kelemen, P., Zimmerman, M., 2005. Observations of Li isotopic variations in the Trinity Ophiolite: evidence for isotopic fractionation by diffusion during mantle melting. Geochimica et Cosmochimica Acta 69, 735-751.

Lytwyn, J.N., Casey, J.F., 1995. The geochemistry of postkinematic mafic dike swarms and subophiolitic metabasites, Pozanti-Karsanti ophiolite, Turkey: Evidence for ridge subduction. Geological Society of America Bulletin 107, 830-850.

Magna, T., Ionov, D.A., Oberli, F., Wiechert, U., 2008. Links between mantle metasomatism and lithium isotopes: Evidence from glass-bearing and cryptically metasomatized xenoliths from Mongolia. Earth and Planetary Science Letters 276, 214-222.

Marschall, H.R., Pogge von Strandmann, P.A.E., Seitz, H.M., Elliott, T., Niu, Y., 2007. The lithium isotopic composition of orogenic eclogites and deep subducted slabs. Earth and Planetary Science Letters 262, 563-580.

Matveev, S., Ballhaus, C., 2002. Role of water in the origin of podiform chromitite deposits. Earth and Planetary Science Letters 203, 235-243.

Melcher, F., Grum, W., Simon, G., Thalhammer, T.V., Stumpfl, E.F., 1997. Petrogenesis of the ophiolitic giant chromite deposits of Kempirsai, Kazakhstan: a study of solid and fluid inclusions in chromite. Journal of Petrology 38, 1419-1458.

Niu, Y.L., 2005. Generation and evolution of basaltic magmas: some basic concepts and a new view on the origin of Mesozoic-Cenozoic basaltic volcanism in eastern China. Geological Journal of China Universities 11, 9-46.

Okay, A.I., 2008. Geology of Turkey: a synopsis. Anschnitt 21, 19-42.

Paktunc, A.D., 1990. Origin of podiform chromite deposits by multistage melting, melt segregation and magma mixing in the upper mantle. Ore Geology Reviews 5, 211-222.

Parkinson, I.J., Hammond, S.J., James, R.H., Rogers, N.W., 2007. High-temperature lithium isotope fractionation: Insights from lithium isotope diffusion in magmatic systems. Earth and Planetary Science Letters 257, 609-621.

Parlak, O., 2000. Geochemistry and significance of mafic dyke swarms in the Pozantı-Karsantı ophiolite (southern Turkey). Turkish Journal of Earth Sciences 9, 29-38.

Parlak, O., Höck, V., Delaloye, M., 2000. Suprasubduction zone origin of the Pozanti-Karsanti ophiolite (southern Turkey) deduced from whole-rock and mineral chemistry of the gabbroic cumulates. Geological Society, London, Special Publications 173, 219-234.

Parlak, O., Höck, V., Delaloye, M., 2002. The supra-subduction zone Pozanti–Karsanti ophiolite, southern Turkey: evidence for high-pressure crystal fractionation of ultramafic cumulates. Lithos 65, 205-224.

Parlak, O., Rızaoğlu, T., Bağci, U., Karaoğlan, F., Hock, V., 2009. Tectonic significance of the geochemistry and petrology of ophiolites in southeast Anatolia, Turkey. Tectonophysics 473, 173-187.

Pearce, J.A., Lippard, S.J., Roberts, S., 1984. Characteristics and tectonic significance of supra-subduction zone ophiolites. Geological Society, London, Special Publications 16, 77-94.

Polat, A., Casey, J. F., Kerrich, R., 1996. Geochemical characteristics of accreted material beneath the Pozanti-Karsanti ophiolite, Turkey: Intra-oceanic detachment, assembly and obduction. Tectonophysics 263, 249-276.

Richter, F., Watson, B., Chaussidon, M., Mendybaev, R., Ruscitto, D., 2014. Lithium isotope fractionation by diffusion in minerals. Part 1: Pyroxenes. Geochimica et Cosmochimica Acta 126, 352-370.

Robertson, A.H.F., 2002. Overview of the genesis and emplacement of Mesozoic ophiolites in the Eastern Mediterranean Tethyan region. Lithos 65, 1-67.

Rollinson, H.R., 2008. The geochemistry of mantle chromitites from the northern part of the Oman ophiolite: inferred parental melt compositions. Contributions to Mineralogy and Petrology 156, 273-288.

Rudnick, R.L., Ionov, D.A., 2007. Lithium elemental and isotopic disequilibrium in minerals from peridotite xenoliths from fareast Russia: product of recent melt/fluid-rock reaction. Earth and Planetary Science Letters 256, 278-293.

Saka, S., Uysal, I., Akmaz, R. M., Kaliwoda, M., Hochleitner, R., 2014. The effects of partial melting, melt–mantle interaction and fractionation on ophiolite generation: Constraints from the late Cretaceous Pozantı-Karsantı ophiolite, southern Turkey. Lithos 202, 300-316.

Seitz, H.M., Brey, G.P., Lahaye, Y., Durali, S., Weyer, S., 2004. Lithium isotopic signatures of peridotite xenoliths and isotopic fractionation at high temperature between olivine and pyroxenes. Chemical Geology 212, 163-177.

Su, B.X., Gu, X.Y., Deloule, E., Zhang, H.F., Li, Q.L., Li, X.H., Vigier, N., Tang, Y.J., Tang, G.Q., Liu, Y., Brewer, A., Mao, Q., Ma, Y.G., 2015. Potential orthopyroxene, clinopyroxene and olivine reference materials for in situ lithium isotope determination. Geostandards and Geoanalytical Research 39, 357-369.

Su, B.X., Zhang, H.F., Deloule, E., Vigier, N., Hu, Y., Tang, Y.J., Xiao, Y., Sakyi, P.A., 2014. Distinguishing silicate and carbonatite mantle metasomatism by using lithium and its isotopes. Chemical Geology 381, 67-77.

Su, B.X., Zhou, M.F., Robinson, P.T., 2016. Extremely large fractionation of Li isotopes in chromitite-bearing mantle sequence. Scientific Reports 6, 22370.

Su, B.X., Chen, C., Bai, Y., Pang, K.N., Qin, K.Z., Sakyi, P.A., 2017. Lithium isotopic composition of Alaskan-type intrusion and its implication. Lithos 286-287, 363-368.

Tang, Y.J., Zhang, H.F., Ying. J.F., 2007. Review of the lithium isotope system as a geochemical tracer. International Geology Review 49, 374-388.

Tang Y.J., Zhang H.F., Deloule E., Su B.X., Ying J.F., Xiao Y., Hu Y. 2012. Slab-derived lithium isotopic signatures in mantle xenoliths from northeastern North China Craton. Lithos, 149, 79-90.

Tang, Y.J., Zhang, H.F., Deloule, E., Su, B.X., Ying, J.F., Santosh, M., Xiao, Y., 2014. Abnormal lithium isotope composition from the ancient lithospheric mantle beneath the North China Craton. Scientific Reports 4, 4274.

Teng, F.Z., McDonough, W.F., Rudnick, R.L., Walker, R.J., Sirbescu, M.L.C., 2006. Lithium isotopic systematics of granites and pegmatites from the Black Hills, South Dakota. American Mineralogist 91, 1488-1498.

Thuizat, R., Whitechurch, H., Montigny, R., Juteau, T., 1981. K-Ar dating of the some infra-ophiolitic metamorphic soles from the eastern Mediterranean: New evidence for intra-oceanic thrusting before obduction. Earth and Planetary Science Letters 52, 302-310.

Tomascak, P.B., Magna, T., Dohmen, R., 2016. Advances in Lithium Isotope Geochemistry. Springer.

Tomascak, P.B., Langmuir, C.H., le Roux, P.J., Shirey, S.B., 2008. Lithium isotopes in global mid-ocean ridge basalts. Geochimica et Cosmochimica Acta 72, 1626-1637.

Tomascak, P.B., Tera, F., Helz, R.T., Walker, R.J., 1999. The absence of lithium isotope fractionation during basalt differentiation: new measurements by multi-collector sector ICP-MS. Geochimica et Cosmochimica Acta 63, 907-910.

Vils, F., Pelletier, L., Kalt, A., Müntener, O., Ludwig, T., 2008. The lithium, boron and beryllium content of serpentinized peridotites from ODP Leg 209 (Sites 1272A and

1274A): implications for lithium and boron budgets of oceanic lithosphere. Geochimica et Cosmochimica Acta 72, 5475-5504.

Vils, F., Tonarini, S., Kalt, A., Seitz, H.M., 2009. Boron, lithium and strontium isotopes as tracers of seawater–serpentinite interaction at Mid-Atlantic ridge, ODP Leg 209. Earth and Planetary Science Letters 286, 414-425.

Woodland, A.B., Seitz, H.M., Yaxley, G.M., 2004. Varying behaviour of Li in metasomatised spinel peridotite xenoliths from western Victoria, Australia. Lithos 75, 55-66.

Xiao, Y., Teng, F.Z., Su, B.X., Hu, Y., Zhou, M.F., Zhu, B., Shi, R.D., Huang, Q.S., Gong, X.H., He, Y.S., 2016. Iron and magnesium isotopic constraints on the origin of chemical heterogeneity in podiform chromitite from the Luobusa ophiolite, Tibet. Geochemistry, Geophysics, Geosystems 17, 940-953.

Xiao, Y., Zhang, H.F., Su, B.X., Zhu, B., Chen, B., Chen, C., Sakyi, P.A., 2017. Partial melting control of lithium concentrations and isotopes in the Cenozoic lithospheric mantle beneath Jiande area, the Cathaysia block of SE China. Chemical Geology 466, 750-761.

Zhou, M.F., Robinson, P., Su, B.X., Gao, J.F., Li, J.W., Yang, J.S., Malpas, J., 2014. Compositions of chromite, associated minerals, and parental magmas of podiform chromite deposits: The role of slab contamination of asthenospheric melts in suprasubduction zone environments. Gondwana Research 26, 262-283.

Zhou, M.F., Robinson, P.T., Malpas, J., Li, Z., 1996. Podiform chromites in the Luobusa ophiolite (southern Tibet): implications for melt-rock interaction and chromite segregation in the upper mantle. Journal of Petrology 37, 3-21.

Zhou, M.F., Sun, M., Keays, R.R., Kerrich, R., 1998. Controls on platinum-group elemental distributions of podiform chromitites: a case study of high-Cr and high-Al chromitites from Chinese orogenic belts. Geochimica et Cosmochimica Acta 62, 677-688.

FIGURE CAPTIONS

Fig. 1. (a) Distribution of ophiolites in Turkey (after Robertson, 2002), (b) geological map (after GDMRE, 2002) and (c) vertical section (after Parlak *et al*., 2009; Dilek & Thy, 2009) of the Pozantı-Karsantı ophiolite.

Fig. 2. Field outcrops and petrological features of the studied samples from mantle-crust transition zone (a-c) and mantle sequence (d) of the Pozantı-Karsantı ophiolite. (a) Field

relations between dunite and wehrlite cumulates; (b) Inter-layered dunite and clinopyroxenite cumulates (1.5 cm diameter of coin used for scale); (c) Inter-layered dunite and chromitite; (d) Podiform chromitite with very thin dunite envelope in harzburgite host.

Fig. 3. Scanned image of a mount showing olivine separates from the Pozantı-Karsantı ophiolitic rocks with an olivine standard for *in situ* Li isotope analysis.

Fig. 4. Diagrams of Fo *vs* NiO (a), MnO (b) and Fe/Mn (c) for olivine in the Pozantı-Karsantı ophiolitic rocks.

Fig. 5. Diagrams of Li (a-c) and δ^7Li (d-f) *vs* Fo, MnO and NiO for olivine in the Pozantı-Karsantı ophiolitic rocks. Symbols are same as in Fig. 4.

Fig. 6. Profile analysis of Li isotopes of serpentine in chromitite sample PK14-41 showing Li and δ^7Li variations with distance away from nodular chromite.

Fig. 7. Variation of Li *vs* δ^7Li for olivine in the Pozantı-Karsantı ophiolitic rocks. Olivine data for the Luobusa (Su *et al*., 2016) and Trinity (Lundstrom *et al*., 2005) ophiolites and Gakkel Ridge peridotites (Gao *et al*., 2011) are plotted for comparison. The δ^7Li ranges of MORB, OIB, arc lavas, eclogite + granulite, altered MORB and marine sediment are from Tomascak *et al*. (2016) and references therein. The trend of Li diffusion or melt percolation is defined on the basis of the Trinity data (Lundstrom *et al*., 2005). Partial melting and fractional crystallization trends are defined on the basis of the incompatibility of Li and its insignificant isotope fractionation during high temperature processes.

Fig. 8 A cartoon of initial subduction showing the diverse materials incorporated into partial melts which penetrate the mantle wedge.

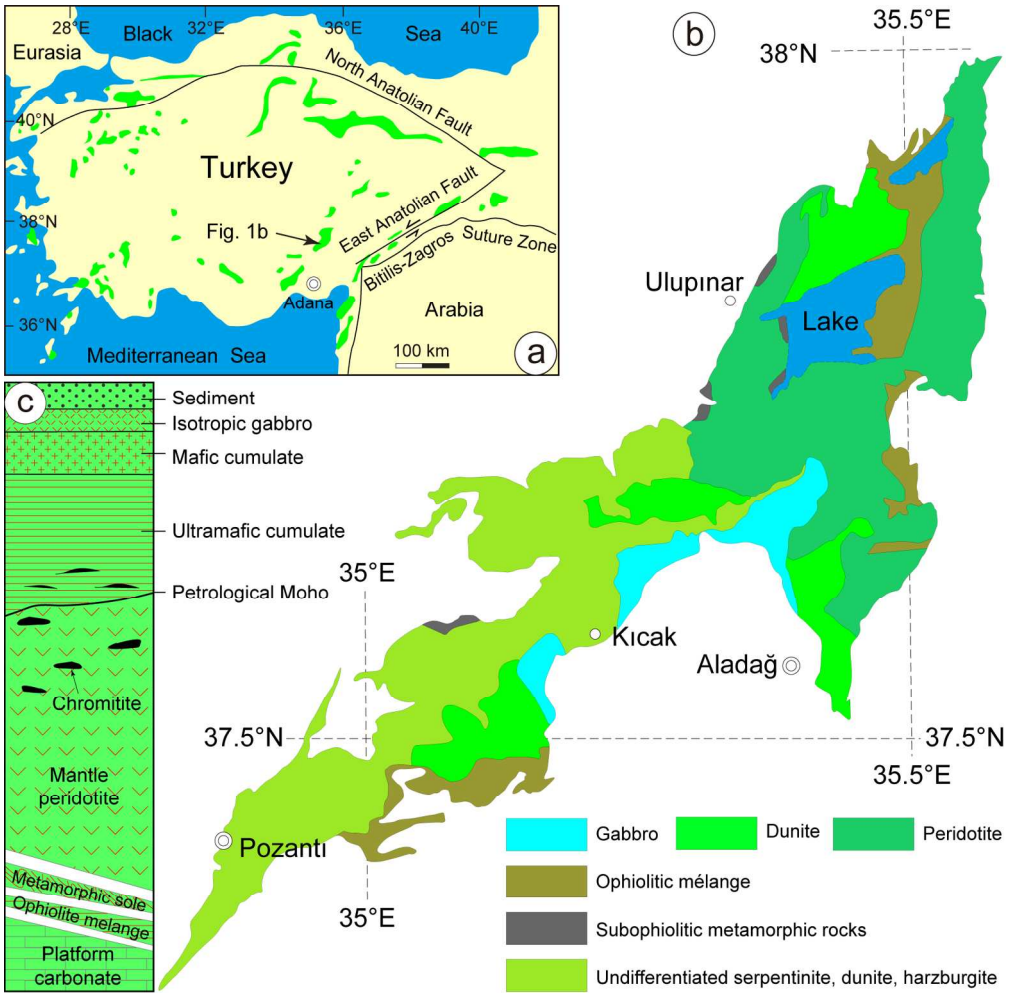

Fig. 1. (a) Distribution of ophiolites in Turkey (after Robertson, 2002), (b) geological map (after GDMRE, 2002) and (c) vertical section (after Parlak et al., 2009; Dilek and Thy, 2009) of the Pozantı-Karsantı ophiolite.

162x159mm (300 x 300 DPI)

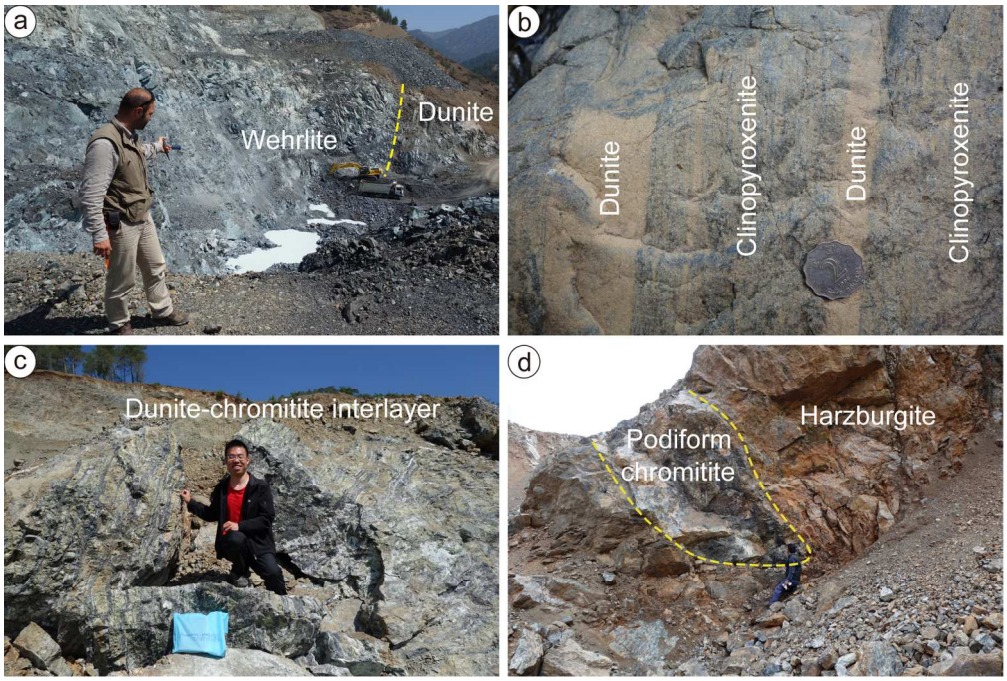

Fig. 2. Field outcrop and petrological features of the studied samples from mantle-crust transition zone (a-c) and mantle sequence (d) of the Pozantı-Karsantı ophiolite. (a) Field relation between dunite and wehrlite cumulates; (b) Inter-layered dunite and clinopyroxenite cumulates (1.5 cm diameter of coin used for scale); (c) Inter-layered dunite and chromitite; (d) Podiform chromitite with very thin dunite envelope in harzburgite host.

160x107mm (300 x 300 DPI)

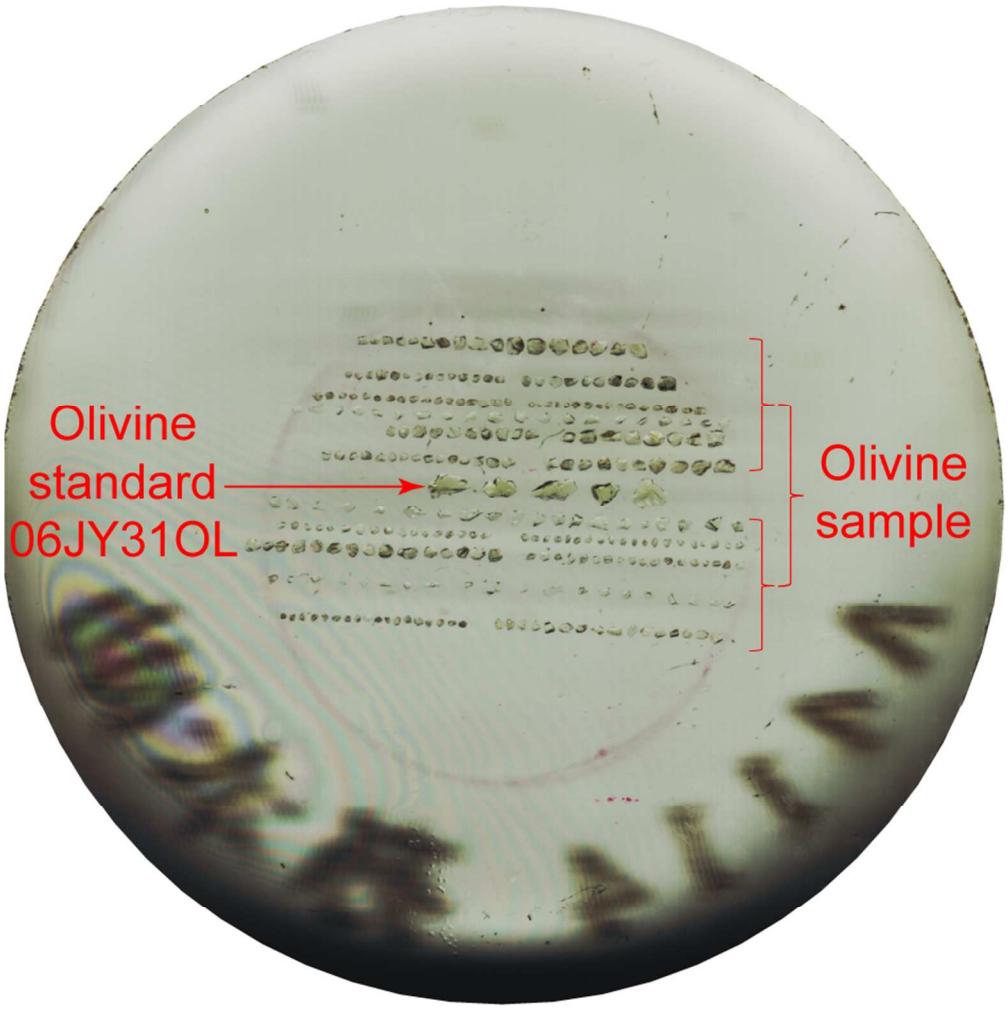

Fig. 3. Scanned image of a mount showing olivine separates in the Pozantı-Karsantı ophiolitic rocks with olivine standard for in situ Li isotope analysis.

79x79mm (300 x 300 DPI)

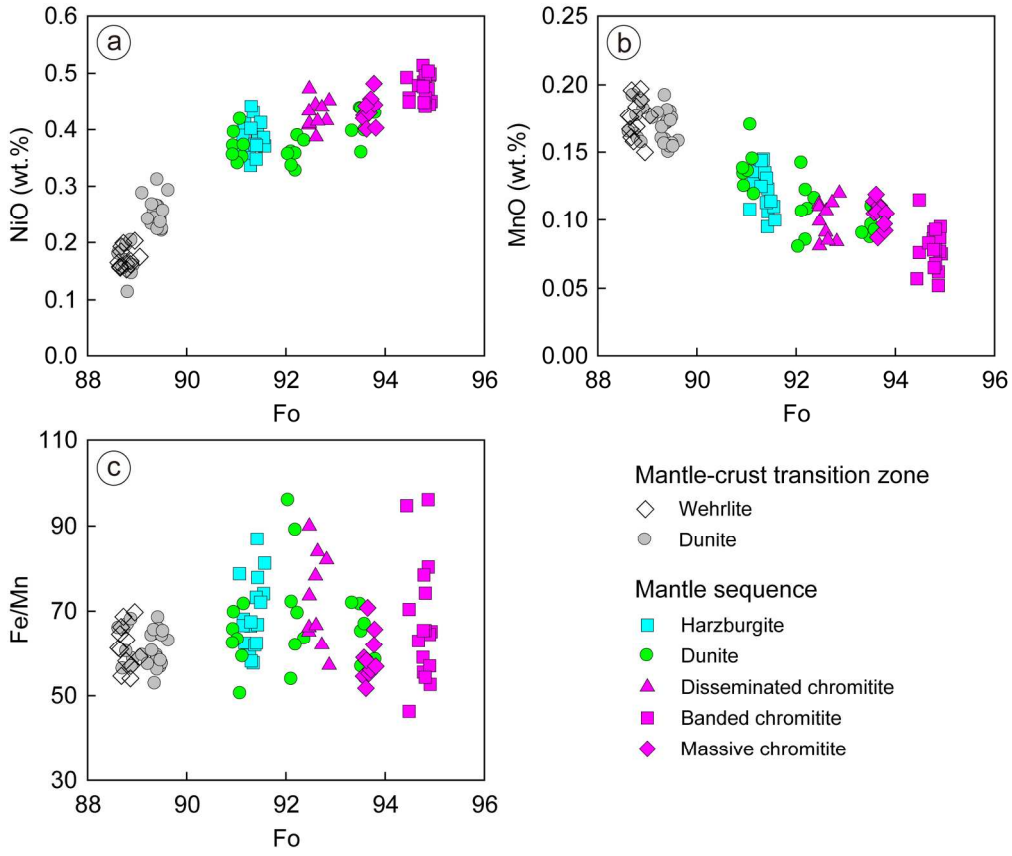

Fig. 4. Diagrams of Fo vs. NiO (a), MnO (b) and Fe/Mn ratio (c) for olivine in the Pozantı-Karsantı ophiolitic rocks.

176x150mm (300 x 300 DPI)

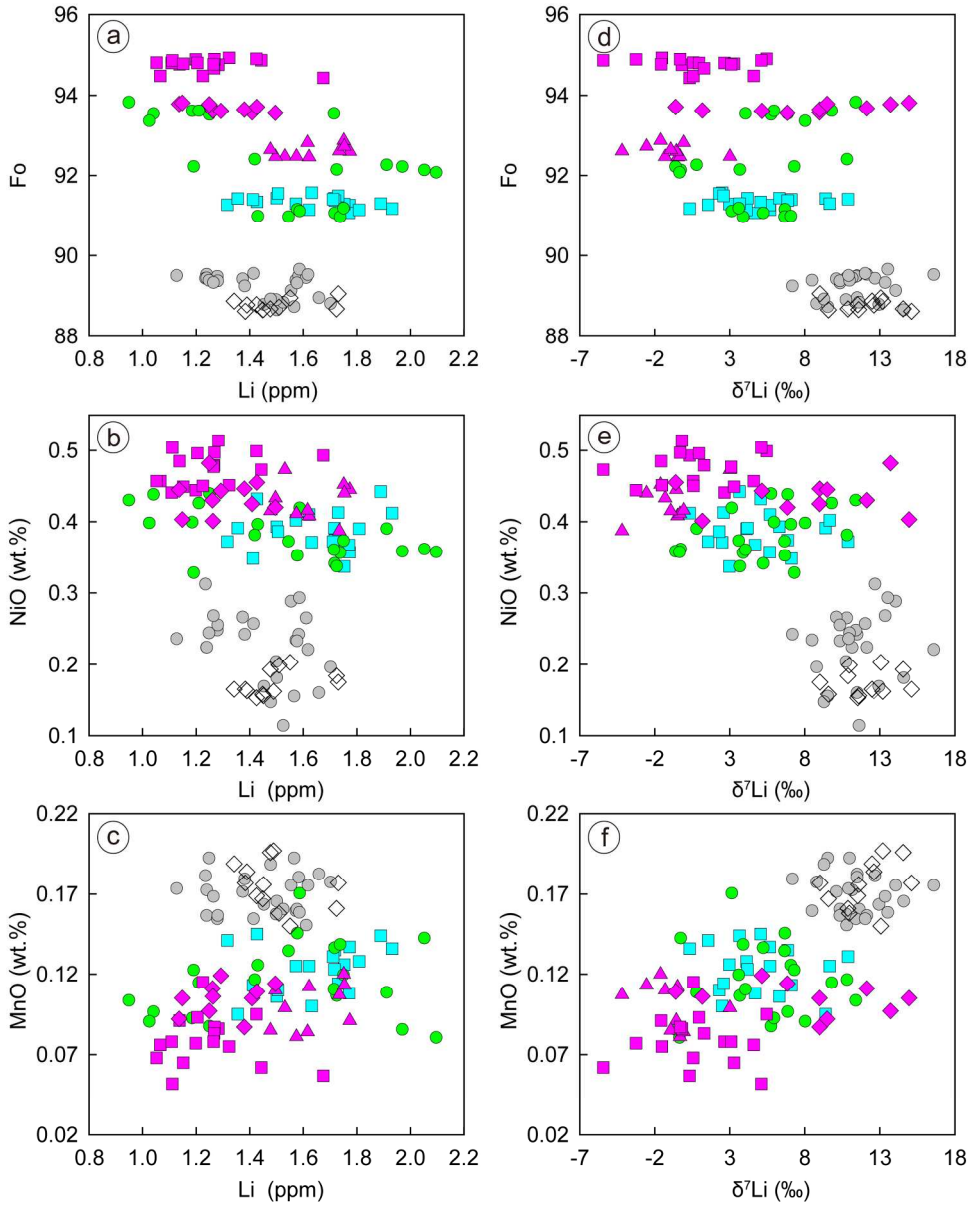

Fig. 5. Diagrams of Li (a-c) and δ7Li (d-f) vs. Fo, MnO and NiO for olivine in the Pozantı-Karsantı ophiolitic rocks. Symbols are same as in Fig. 4.

179x224mm (300 x 300 DPI)

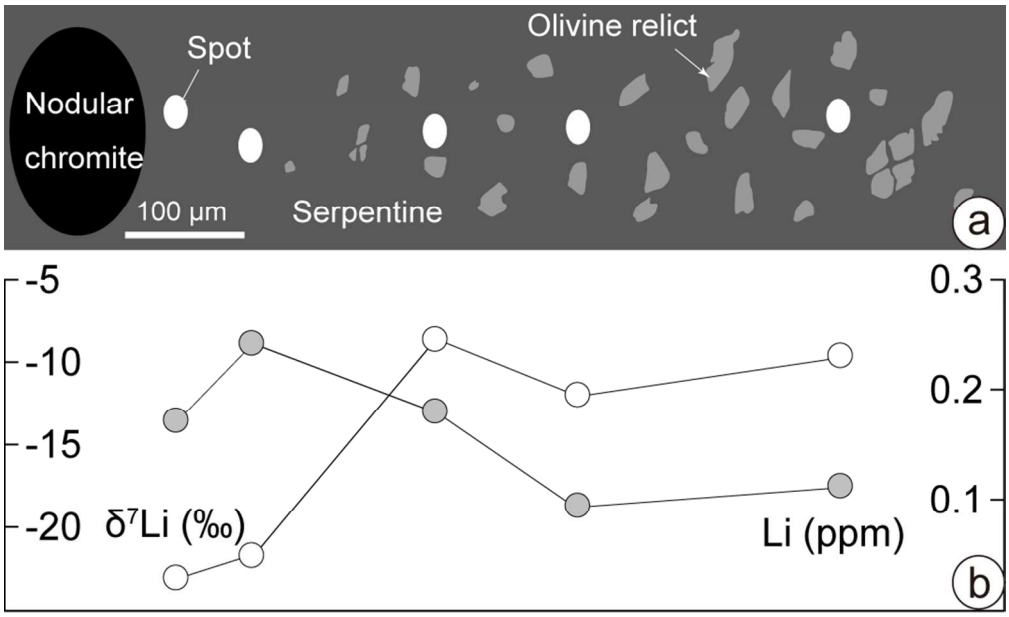

Fig. 6. Profile analysis of Li isotopes of serpentine in chromitite sample PK14-41 showing Li and δ7Li variations at a distance away from nodular chromite.

90x55mm (300 x 300 DPI)

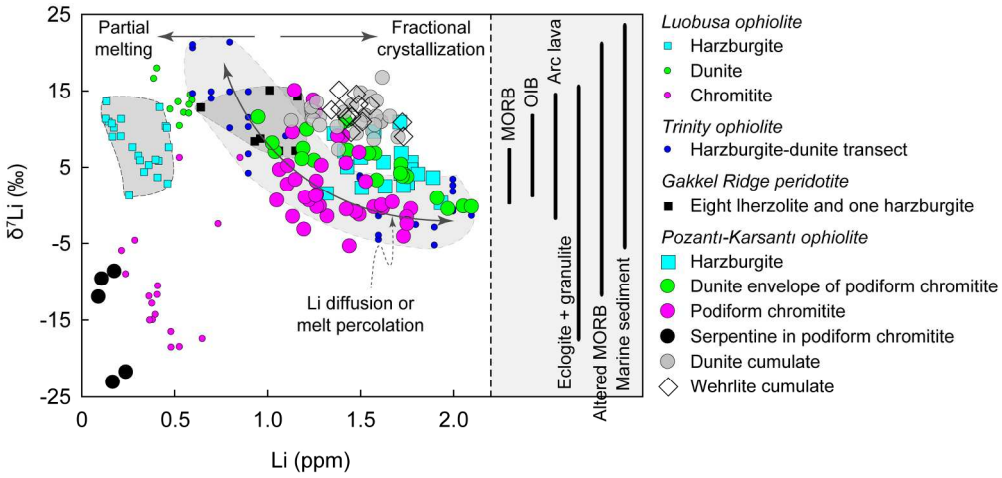

Fig. 7. Diagram of Li vs. δ7Li for olivine in the Pozantı-Karsantı ophiolitic rocks. Olivine data of the Luobusa (Su et al., 2016) and Trinity (Lundstrom et al., 2005) ophiolites and Gakkel Ridge peridotites (Gao et al., 2011) are plotted for comparison. The δ7Li ranges of MORB, OIB, arc lava, eclogite + granulite, altered MORB and marine sediment are from Tomascak et al. (2016) and references therein. The trend of Li diffusion or melt percolation is defined on the basis of the Trinity data (Lundstrom et al., 2005). Partial melting and fractional crystallization trends are defined on the basis of incompatibility of element Li and insignificant isotope fractionation during these high temperature processes.

195x92mm (300 x 300 DPI)

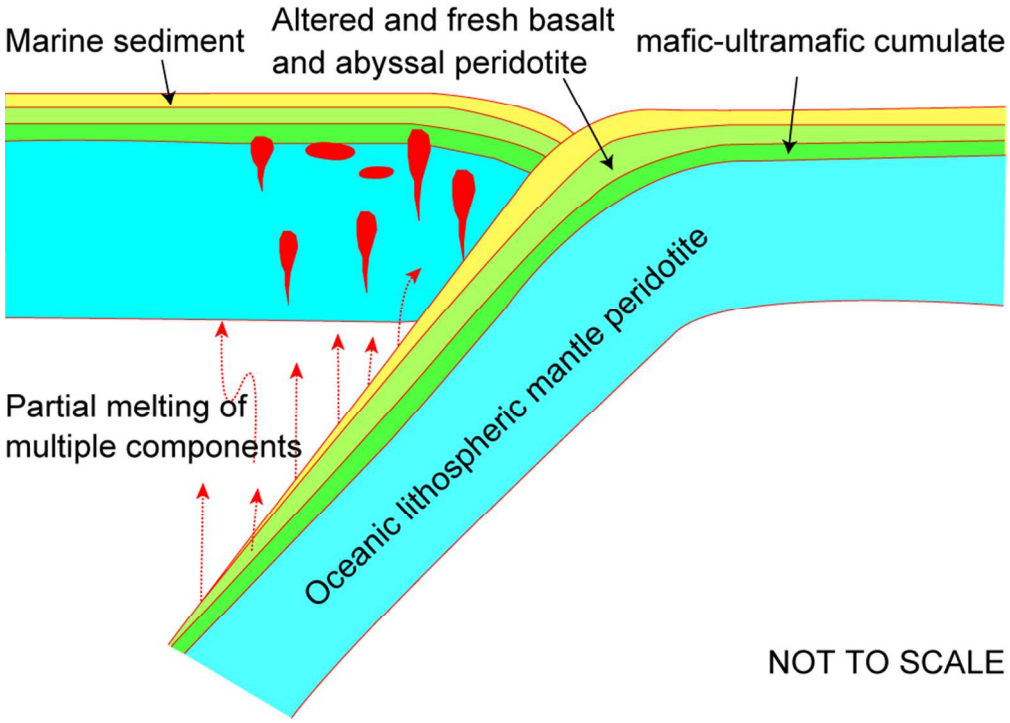

Fig. 8 A cartoon of initial subduction showing diverse materials incorporated into partial melts to penetrate mantle wedge.

87x62mm (300 x 300 DPI)

Table 1 GPS locations of the studied samples collected from the Pozantı-Karsantı ophiolite, south Turkey.

Sample	Rock type	Latitude	Longitude	Comment
PK14-35	Harzburgite	37°37′45″N	35°29′05 E	Mantle harzburgite hosting chromitite
PK14-40	Harzburgite	37°38′58″N	35°29′03″E	Mantle harzburgite hosting chromitite
PK14-05	Harzburgite	37°39′58″N	35°25′13″E	Mantle harzburgite hosting chromitite
PK14-38	Dunite	37°38′58″N	35°29′03″E	Mantle dunite envelope of chromitite
PK14-20	Dunite	37°36′38″N	35°28′43″E	Mantle dunite envelope of chromitite
PK14-54	Dunite	37°36′28″N	35°26′11″E	Mantle dunite envelope of chromitite
PK14-16	Dunite	37°37′06″N	35°23′39″E	Cumulate in mantle-crust transition zone
PK14-70	Dunite	37°36′14″N	35°24′24″E	Cumulate in mantle-crust transition zone
PK14-72	Dunite	37°36′14″N	35°24′24″E	Cumulate in mantle-crust transition zone
PK14-15	Wehrlite	37°37′06″N	35°23′39″E	Cumulate in mantle-crust transition zone
PK14-46	Disseminated chromitite	37°38′58″N	35°29′03″E	Chromitite body in mantle sequence
PK14-52	Banded chromitite	37°36′28″N	35°26′11″E	Chromitite body in mantle sequence
PK14-75	Banded chromitite	37°36′28″N	35°26′11″E	Chromitite body in mantle sequence
PK14-09	Massive chromitite	37°39′58″N	35°25′13″E	Chromitite body in mantle sequence
PK14-41	Nodular chromitite	37°38′58″N	35°29′03″E	Chromitite body in mantle sequence

Table 2 Li concentration, δ^7Li and major oxide compositions of olivine in the Pozantı-Karsantı ophiolite, south Turkey.

Sample@Spot	Comment	δ^7Li	1se	Li	1σ	SiO_2	TiO_2	Al_2O_3	Cr_2O_3	FeO	MnO	MgO	CaO	Na_2O	K_2O	NiO	Total	Fo	Fe/Mn
PK14-35 Ol@1	Grain 1	5.67	0.85	1.62	0.72	40.6	0.00	0.01	0.00	8.63	0.13	49.3	0.01	0.00	0.00	0.41	99.2	91.1	68.1
PK14-35 Ol@2	Grain 2	5.66	0.80	1.77	0.72	40.6	0.00	0.00	0.00	8.49	0.14	49.3	0.02	0.02	0.01	0.36	98.9	91.3	61.1
PK14-35 Ol@3	Grain 3	4.69	0.88	1.77	0.78	40.8	0.01	0.00	0.00	8.62	0.11	48.8	0.03	0.02	0.02	0.37	98.8	91.1	78.7
PK14-35 Ol@4	Grain 4	1.55	0.99	1.32	0.54	40.7	0.02	0.00	0.03	8.51	0.14	49.4	0.02	0.00	0.00	0.37	99.3	91.3	59.5
PK14-35 Ol@5	Grain 5	2.98	0.80	1.75	0.71	40.4	0.00	0.00	0.00	8.50	0.13	49.5	0.03	0.00	0.02	0.34	98.9	91.3	66.5
PK14-35 Ol@6	Grain 6	4.12	0.73	1.81	0.77	40.8	0.00	0.00	0.01	8.64	0.13	49.4	0.03	0.00	0.00	0.39	99.4	91.1	66.6
PK14-35 Ol@7	Grain 7	0.33	0.81	1.93	0.77	40.5	0.04	0.01	0.01	8.62	0.14	49.4	0.02	0.00	0.00	0.41	99.2	91.2	62.5
PK14-40 Ol@1	Grain 1	4.18	0.97	1.72	0.68	40.9	0.00	0.00	0.00	8.34	0.12	49.4	0.01	0.00	0.01	0.39	99.2	91.4	66.9
PK14-40 Ol@2	Grain 2	9.39	0.92	1.36	0.66	40.8	0.00	0.00	0.01	8.37	0.10	49.6	0.01	0.04	0.01	0.39	99.4	91.4	86.9
PK14-40 Ol@3	Grain 3	6.30	0.83	1.50	0.61	40.5	0.00	0.00	0.00	8.37	0.11	49.6	0.03	0.01	0.00	0.39	99.0	91.4	77.8
PK14-40 Ol@4	Grain 4	5.05	0.93	1.43	0.63	40.3	0.00	0.00	0.00	8.49	0.15	49.8	0.03	0.00	0.00	0.43	99.1	91.3	57.8
PK14-40 Ol@5	Grain 5	2.50	0.83	1.63	0.70	40.6	0.00	0.00	0.00	8.24	0.10	49.7	0.04	0.00	0.00	0.37	99.1	91.6	81.2
PK14-40 Ol@6	Grain 6	2.30	0.85	1.51	0.60	40.2	0.01	0.00	0.00	8.26	0.11	49.7	0.03	0.03	0.00	0.39	98.8	91.6	74.1
PK14-40 Ol@7	Grain 7	7.11	0.78	1.41	0.56	40.4	0.00	0.00	0.03	8.39	0.11	49.5	0.03	0.00	0.01	0.35	98.9	91.4	73.2
PK14-05 Ol@1	Grain 1	2.58	0.80	1.73	1.02	40.9	0.00	0.00	0.00	8.34	0.11	49.8	0.02	0.00	0.02	0.41	99.6	91.5	72.1
PK14-05 Ol@2	Grain 2	6.87	0.75	1.72	1.09	40.7	0.00	0.00	0.00	8.49	0.14	49.9	0.02	0.01	0.01	0.37	99.7	91.4	62.0
PK14-05 Ol@3	Grain 3	10.88	0.67	1.71	1.31	41.1	0.00	0.00	0.00	8.30	0.13	49.0	0.02	0.00	0.00	0.37	100	91.4	62.5
PK14-05 Ol@4	Grain 4	9.66	0.66	1.57	1.25	41.0	0.00	0.05	0.01	8.55	0.13	49.8	0.03	0.00	0.00	0.40	100	91.3	67.5
PK14-05 Ol@5	Grain 5	3.64	0.54	1.89	1.27	41.2	0.00	0.00	0.00	8.50	0.14	49.5	0.02	0.00	0.00	0.44	99.9	91.3	58.2
PK14-16 Ol@1	Grain 1 rim	13.00	0.72	1.46	0.82	40.4	0.00	0.00	0.01	10.9	0.16	47.9	0.04	0.00	0.02	0.17	99.6	88.8	66.0
PK14-16 Ol@2	Grain 1 core	14.65	0.72	1.50	0.85	40.8	0.00	0.00	0.00	11.0	0.17	47.8	0.05	0.01	0.01	0.18	100	88.6	66.0
PK14-16 Ol@3	Grain 2	11.54	0.59	1.66	0.94	40.3	0.01	0.00	0.00	10.8	0.18	48.3	0.03	0.00	0.00	0.16	99.7	88.9	58.6
PK14-16 Ol@4	Grain 3 rim	8.84	0.72	1.70	0.94	39.8	0.02	0.00	0.00	10.8	0.18	47.7	0.02	0.00	0.01	0.20	98.8	88.8	60.4
PK14-16 Ol@5	Grain 3 mantle	9.58	0.80	1.57	0.90	39.6	0.00	0.00	0.01	11.0	0.19	47.9	0.04	0.24	0.05	0.15	99.2	88.7	56.3
PK14-16 Ol@6	Grain 3 core	11.67	0.75	1.53	0.88	39.9	0.01	0.00	0.00	10.8	0.16	47.9	0.01	0.01	0.00	0.11	99.0	88.8	66.9
PK14-16 Ol@7	Grain 3 core	10.80	0.71	1.50	0.84	40.0	0.00	0.00	0.00	10.8	0.16	48.1	0.00	0.00	0.01	0.20	99.4	88.9	68.0
PK14-16 Ol@8	Grain 3 mantle	9.33	0.77	1.48	0.80	39.8	0.02	0.00	0.00	10.8	0.19	48.1	0.02	0.00	0.00	0.15	99.2	88.9	56.8
PK14-70 Ol@1	Grain 1	14.12	0.60	1.56	1.18	40.7	0.02	0.00	0.01	10.6	0.18	48.0	0.13	0.01	0.00	0.29	99.9	89.1	59.5

PK14-70 Ol@2	Grain 2	8.53	0.76	1.58	1.04	40.9	0.00	0.00	0.01	10.4	0.16	48.6	0.13	0.01	0.00	0.23	100	89.4	64.5
PK14-70 Ol@3	Grain 3 rim	11.54	0.70	1.59	1.09	40.6	0.00	0.01	0.03	10.3	0.18	48.9	0.12	0.00	0.00	0.24	100	89.5	56.7
PK14-70 Ol@4	Grain 3 mantle	10.85	0.68	1.61	1.02	40.5	0.01	0.00	0.01	10.4	0.15	48.9	0.10	0.01	0.01	0.26	100	89.4	68.4
PK14-70 Ol@5	Grain 3 core	10.41	0.52	1.58	0.95	40.2	0.00	0.00	0.03	10.4	0.16	48.3	0.12	0.03	0.00	0.23	99.5	89.3	64.2
PK14-70 Ol@6	Grain 4 rim	13.59	0.72	1.59	0.98	40.3	0.00	0.00	0.02	10.1	0.16	48.5	0.12	0.00	0.00	0.29	99.5	89.6	62.9
PK14-70 Ol@7	Grain 4 core	16.65	0.69	1.62	0.94	40.7	0.01	0.00	0.00	10.2	0.18	48.3	0.11	0.01	0.01	0.22	99.7	89.5	57.4
PK14-38 Ol@1	Grain 1	6.73	0.88	1.58	0.64	41.0	0.02	0.00	0.01	8.70	0.15	49.7	0.02	0.02	0.00	0.35	100	91.1	59.2
PK14-38 Ol@2	Grain 2	6.71	0.84	1.55	0.70	40.9	0.03	0.00	0.01	8.92	0.13	49.7	0.04	0.02	0.01	0.37	100	90.9	65.6
PK14-38 Ol@3	Grain 3	3.19	0.87	1.59	0.66	40.7	0.00	0.00	0.00	8.70	0.17	49.4	0.05	0.00	0.00	0.42	99.4	91.1	50.5
PK14-38 Ol@4	Grain 4	5.28	0.94	1.72	0.77	40.8	0.00	0.00	0.00	8.73	0.14	49.2	0.03	0.00	0.00	0.34	99.2	91.0	63.3
PK14-38 Ol@5	Grain 5	7.12	0.84	1.43	0.60	40.9	0.00	0.00	0.00	8.83	0.13	49.3	0.03	0.02	0.01	0.40	99.7	91.0	69.6
PK14-38 Ol@6	Grain 6 rim	3.94	0.96	1.74	0.88	40.8	0.02	0.00	0.00	8.73	0.14	48.6	0.05	0.00	0.01	0.36	98.8	90.9	62.3
PK14-38 Ol@7	Grain 6 core	3.66	0.83	1.75	0.89	40.4	0.02	0.00	0.00	8.64	0.12	49.5	0.04	0.02	0.01	0.37	99.1	91.2	71.6
PK14-20 Ol@1	Grain 1	-0.22	0.68	2.06	1.07	41.1	0.00	0.00	0.00	7.75	0.14	50.3	0.05	0.00	0.00	0.36	99.8	92.1	53.8
PK14-20 Ol@2	Grain 2	0.85	0.87	1.91	0.77	41.2	0.03	0.00	0.00	7.61	0.11	50.2	0.04	0.03	0.00	0.39	99.7	92.2	69.4
PK14-20 Ol@3	Grain 3	-0.57	0.75	1.97	0.90	40.9	0.01	0.00	0.02	7.67	0.09	50.4	0.03	0.00	0.00	0.36	99.4	92.2	89.0
PK14-20 Ol@4	Grain 4	10.86	0.80	1.42	0.66	41.1	0.01	0.00	0.02	7.46	0.12	50.2	0.04	0.00	0.00	0.38	99.4	92.4	63.4
PK14-20 Ol@5	Grain 5	7.36	0.86	1.19	0.53	41.1	0.00	0.00	0.00	7.66	0.12	50.3	0.07	0.00	0.01	0.33	99.6	92.2	61.9
PK14-20 Ol@6	Grain 6	-0.29	0.86	2.10	1.03	40.9	0.00	0.00	0.00	7.79	0.08	50.1	0.03	0.02	0.01	0.36	99.3	92.1	96.0
PK14-20 Ol@7	Grain 7	3.72	0.76	1.73	0.85	40.5	0.03	0.00	0.02	7.74	0.11	50.3	0.03	0.04	0.00	0.34	99.1	92.1	72.0
PK14-54 Ol@1	Grain 1	5.80	0.86	1.25	0.51	41.3	0.00	0.00	0.03	6.31	0.09	50.4	0.08	0.03	0.02	0.44	98.7	93.5	71.5
PK14-54 Ol@2	Grain 2	6.92	0.91	1.04	0.46	40.7	0.02	0.01	0.00	6.35	0.10	50.9	0.05	0.03	0.00	0.44	98.6	93.5	65.2
PK14-54 Ol@3	Grain 3	8.08	1.12	1.03	0.36	41.2	0.00	0.00	0.00	6.56	0.09	51.1	0.10	0.00	0.01	0.40	99.4	93.3	71.8
PK14-54 Ol@4	Grain 4	6.00	1.12	1.19	0.47	41.1	0.00	0.00	0.00	6.24	0.09	50.6	0.08	0.00	0.01	0.40	98.6	93.6	66.9
PK14-54 Ol@5	Grain 5	9.85	1.05	1.21	0.54	41.2	0.02	0.00	0.00	6.26	0.11	50.8	0.03	0.01	0.01	0.43	98.9	93.6	54.1
PK14-54 Ol@6	Grain 6	4.10	0.80	1.72	0.66	41.0	0.00	0.00	0.05	6.34	0.11	50.9	0.06	0.00	0.01	0.36	98.9	93.5	56.8
PK14-54 Ol@7	Grain 7	11.45	1.08	0.95	0.43	41.0	0.00	0.00	0.00	6.11	0.10	51.4	0.04	0.00	0.00	0.43	99.1	93.8	58.5
PK14-72 Ol@1	Grain 1 rim	12.19	0.93	1.24	0.67	40.3	0.01	0.00	0.02	10.2	0.16	48.2	0.10	0.01	0.00	0.22	99.1	89.5	64.2
PK14-72 Ol@02	Grain 1 mantle	11.47	0.95	1.28	0.55	40.4	0.01	0.01	0.00	10.3	0.15	48.4	0.11	0.02	0.00	0.25	99.6	89.5	65.7
PK14-72 Ol@03	Grain 1 core	12.74	0.89	1.24	0.53	40.2	0.01	0.00	0.00	10.3	0.18	48.3	0.12	0.01	0.01	0.31	99.6	89.4	56.1

PK14-72 Ol@04	Grain 1 mantle	10.16	0.82	1.38	0.57	40.2	0.04	0.00	0.00	10.3	0.17	48.3	0.12	0.01	0.02	0.27	99.5	89.4	59.5
PK14-72 Ol@05	Grain 2 rim	10.39	0.88	1.28	0.63	40.7	0.00	0.00	0.00	10.4	0.16	48.3	0.11	0.03	0.00	0.25	99.9	89.4	65.5
PK14-72 Ol@06	Grain 2 mantle	11.20	0.89	1.24	0.62	40.4	0.01	0.00	0.00	10.3	0.17	48.2	0.11	0.03	0.02	0.22	99.4	89.4	58.8
PK14-72 Ol@07	Grain 2 mantle	11.04	0.78	1.25	0.57	40.5	0.00	0.00	0.00	10.3	0.19	48.0	0.14	0.02	0.02	0.24	99.5	89.4	52.8
PK14-72 Ol@08	Grain 2 core	13.41	0.92	1.27	0.46	40.4	0.00	0.00	0.00	10.3	0.17	47.9	0.14	0.01	0.02	0.27	99.2	89.3	60.5
PK14-72 Ol@09	Grain 3	7.23	0.83	1.38	0.59	40.7	0.00	0.00	0.00	10.4	0.18	47.9	0.10	0.01	0.00	0.24	99.5	89.2	57.3
PK14-72 Ol@10	Grain 4	12.08	0.90	1.42	0.56	39.7	0.00	0.00	0.00	10.2	0.15	48.4	0.11	0.01	0.00	0.26	98.9	89.5	65.2
PK14-72 Ol@11	Grain 5	10.97	1.09	1.13	0.52	40.0	0.02	0.00	0.00	10.2	0.17	48.3	0.11	0.03	0.02	0.24	99.1	89.5	58.2
PK14-15 Ol@1	Grain 1	12.60	0.93	1.39	0.60	40.2	0.00	0.00	0.00	10.9	0.18	47.7	0.02	0.01	0.01	0.16	99.1	88.8	58.2
PK14-15 Ol@2	Grain 2	12.48	1.06	1.34	0.60	40.6	0.02	0.00	0.02	10.9	0.19	48.4	0.02	0.01	0.00	0.17	99.1	88.9	57.0
PK14-15 Ol@3	Grain 3	10.96	1.04	1.51	0.72	40.5	0.01	0.00	0.02	11.0	0.16	48.1	0.01	0.00	0.01	0.20	100	88.7	68.7
PK14-15 Ol@4	Grain 4 rim	10.87	0.98	1.72	0.70	40.3	0.00	0.00	0.02	10.8	0.16	47.1	0.05	0.00	0.01	0.18	98.6	88.7	66.3
PK14-15 Ol@5	Grain 4 mantle	11.59	0.99	1.45	0.67	40.2	0.00	0.00	0.00	10.9	0.18	47.3	0.04	0.01	0.02	0.16	98.8	88.7	61.0
PK14-15 Ol@6	Grain 4 core	14.56	0.84	1.48	0.64	40.2	0.04	0.00	0.00	10.9	0.20	47.3	0.05	0.01	0.02	0.19	98.8	88.7	54.6
PK14-15 Ol@7	Grain 4 mantle	9.57	0.94	1.45	0.65	40.4	0.00	0.00	0.00	10.9	0.17	47.5	0.03	0.00	0.00	0.16	99.2	88.7	64.6
PK14-15 Ol@8	Grain 4 rim	11.53	1.00	1.43	0.58	40.4	0.01	0.00	0.00	10.8	0.17	47.7	0.03	0.04	0.00	0.15	99.3	88.8	63.3
PK14-15 Ol@9	Grain 5	13.20	0.79	1.49	0.64	40.3	0.00	0.00	0.00	10.8	0.20	47.9	0.02	0.02	0.01	0.16	99.4	88.9	54.1
PK14-15 Ol@10	Grain 6	9.01	0.91	1.73	0.70	40.2	0.01	0.00	0.01	10.6	0.18	48.0	0.02	0.00	0.00	0.18	99.3	89.1	59.1
PK14-15 Ol@11	Grain 7	13.07	0.87	1.55	0.57	40.1	0.03	0.00	0.00	10.6	0.15	47.5	0.04	0.01	0.00	0.20	98.7	89.0	69.7
PK14-15 Ol@12	Grain 8	15.11	0.85	1.38	0.46	40.2	0.03	0.00	0.03	11.0	0.18	47.6	0.02	0.00	0.01	0.17	99.3	88.6	61.3
PK14-46 Ol@1	Grain 1	-0.48	0.73	1.62	0.61	41.1	0.00	0.00	0.00	7.40	0.11	50.4	0.00	0.02	0.02	0.41	99.5	92.5	65.1
PK14-46 Ol@2	Grain 2	3.01	0.82	1.53	0.58	40.4	0.00	0.01	0.01	7.39	0.10	50.4	0.02	0.00	0.00	0.47	98.8	92.5	73.6
PK14-46 Ol@3	Grain 3	-0.32	0.71	1.57	0.58	40.7	0.00	0.00	0.01	7.39	0.08	50.5	0.03	0.00	0.00	0.41	99.1	92.5	90.0
PK14-46 Ol@4	Grain 4	-0.57	0.75	1.77	0.63	41.0	0.00	0.00	0.00	7.22	0.09	50.1	0.03	0.00	0.00	0.45	99.0	92.6	78.2
PK14-46 Ol@5	Grain 5	-1.31	0.91	1.50	0.50	40.6	0.00	0.00	0.02	7.38	0.11	50.3	0.06	0.02	0.00	0.43	99.0	92.5	66.2
PK14-46 Ol@6	Grain 6 rim	-0.07	0.79	1.62	0.59	41.2	0.00	0.00	0.01	6.98	0.08	50.1	0.02	0.01	0.00	0.42	98.9	92.8	82.0
PK14-46 Ol@7	Grain 6 mantle	-1.62	0.70	1.75	0.68	41.2	0.00	0.00	0.01	6.95	0.12	50.3	0.03	0.01	0.01	0.45	99.2	92.9	57.1
PK14-46 Ol@8	Grain 6 core	-4.19	0.74	1.73	0.72	41.2	0.01	0.00	0.00	7.23	0.11	50.3	0.03	0.00	0.01	0.39	99.3	92.6	66.6
PK14-46 Ol@9	Grain 6 mantle	-2.55	0.74	1.75	0.71	41.0	0.00	0.00	0.00	7.11	0.11	50.3	0.03	0.00	0.01	0.44	99.0	92.7	62.0
PK14-46 Ol@10	Grain 7	-0.93	0.80	1.48	0.57	40.7	0.03	0.00	0.00	7.23	0.09	50.6	0.04	0.00	0.00	0.42	99.1	92.6	83.9

PK14-52 Ol@1	Grain 1	0.32	0.78	1.67	0.71	41.4	0.00	0.00	0.00	5.48	0.06	51.6	0.07	0.00	0.01	0.49	99.1	94.4	94.7
PK14-52 Ol@2	Grain 2	-1.52	1.02	1.32	0.52	41.5	0.00	0.00	0.00	4.96	0.08	51.6	0.05	0.01	0.00	0.45	98.7	94.9	65.2
PK14-52 Ol@3	Grain 3	-1.58	0.92	1.14	0.44	41.6	0.00	0.00	0.00	5.13	0.09	51.6	0.08	0.01	0.02	0.49	99.0	94.8	55.6
PK14-52 Ol@4	Grain 4	-0.19	0.94	1.28	0.51	41.0	0.00	0.00	0.00	5.15	0.09	51.8	0.08	0.00	0.01	0.51	98.6	94.8	59.1
PK14-52 Ol@5	Grain 5	4.60	0.89	1.07	0.43	41.2	0.01	0.00	0.00	5.43	0.08	51.6	0.09	0.00	0.01	0.46	98.8	94.5	70.4
PK14-52 Ol@6	Grain 6	-3.25	1.01	1.20	0.52	41.2	0.00	0.00	0.00	5.04	0.08	52.0	0.06	0.00	0.02	0.44	98.9	94.9	64.5
PK14-52 Ol@7	Grain 7	-5.43	0.88	1.44	0.69	41.4	0.00	0.00	0.02	5.05	0.06	51.9	0.08	0.01	0.01	0.47	99.0	94.9	80.3
PK14-52 Ol@8	Grain 8	0.56	1.03	1.05	0.42	40.9	0.02	0.00	0.02	5.12	0.07	51.9	0.09	0.03	0.01	0.46	98.6	94.8	74.2
PK14-52 Ol@9	Grain 9	-0.31	0.97	1.27	0.61	41.0	0.01	0.00	0.01	5.03	0.09	52.0	0.08	0.00	0.01	0.50	98.7	94.9	57.0
PK14-52 Ol@10	Grain 10	0.57	0.99	1.22	0.53	41.1	0.00	0.00	0.00	5.40	0.12	51.4	0.04	0.00	0.01	0.45	98.5	94.5	46.3
PK14-75 Ol@1	Grain 1	5.46	0.71	1.42	1.16	41.3	0.00	0.00	0.00	5.08	0.10	52.6	0.08	0.00	0.00	0.50	99.6	94.9	52.7
PK14-75 Ol@2	Grain 2	0.94	0.79	1.21	0.77	41.6	0.00	0.00	0.00	5.13	0.09	52.0	0.08	0.00	0.00	0.50	99.4	94.8	54.3
PK14-75 Ol@3	Grain 3 rim	2.65	0.93	1.11	0.76	41.3	0.04	0.00	0.03	5.18	0.08	52.5	0.08	0.02	0.01	0.44	99.6	94.8	65.5
PK14-75 Ol@4	Grain 3 core	5.11	0.85	1.11	0.70	41.4	0.00	0.00	0.02	5.07	0.05	52.1	0.08	0.00	0.00	0.50	99.2	94.9	96.2
PK14-75 Ol@5	Grain 4 rim	3.28	0.85	1.15	0.76	41.7	0.00	0.00	0.00	5.17	0.07	52.2	0.10	0.00	0.01	0.45	99.8	94.8	78.4
PK14-75 Ol@6	Grain 4 mantle	1.29	0.78	1.27	0.68	41.6	0.04	0.00	0.00	5.30	0.08	52.3	0.08	0.00	0.02	0.48	100	94.7	63.0
PK14-75 Ol@7	Grain 4 core	3.09	0.68	1.27	0.69	41.4	0.00	0.00	0.00	5.18	0.08	52.1	0.12	0.03	0.02	0.48	99.4	94.8	65.5
PK14-09 Ol@1	Grain 1 rim	8.98	0.62	1.41	0.90	41.2	0.00	0.00	0.00	6.28	0.11	50.8	0.11	0.01	0.00	0.43	99.0	93.6	59.0
PK14-09 Ol@2	Grain 1 mantle	8.99	0.90	1.38	0.80	40.6	0.00	0.00	0.00	6.24	0.09	51.1	0.09	0.00	0.01	0.45	98.7	93.6	70.8
PK14-09 Ol@3	Grain 1 core	6.84	0.77	1.50	0.93	40.8	0.01	0.00	0.02	6.31	0.11	50.9	0.13	0.00	0.00	0.42	98.8	93.6	54.6
PK14-09 Ol@4	Grain 2	12.13	0.82	1.26	0.79	41.0	0.00	0.00	0.00	6.22	0.11	51.2	0.11	0.00	0.00	0.43	99.1	93.7	55.3
PK14-09 Ol@5	Grain 3	9.48	0.70	1.14	0.59	40.3	0.00	0.00	0.02	6.13	0.09	51.4	0.12	0.17	0.05	0.45	98.8	93.8	65.7
PK14-09 Ol@6	Grain 4	-0.61	0.68	1.43	0.72	41.1	0.00	0.00	0.00	6.20	0.11	51.3	0.07	0.00	0.01	0.46	99.2	93.7	56.1
PK14-09 Ol@7	Grain 5	1.17	0.81	1.26	0.65	41.5	0.01	0.00	0.01	6.27	0.11	51.1	0.10	0.01	0.00	0.40	99.6	93.6	58.3
PK14-09 Ol@8	Grain 6	5.14	0.98	1.29	0.78	41.2	0.02	0.00	0.00	6.25	0.12	50.9	0.07	0.02	0.00	0.44	99.1	93.6	51.8
PK14-09 Ol@9	Grain 7 rim	14.95	1.00	1.15	0.60	40.9	0.01	0.00	0.00	6.06	0.11	51.1	0.09	0.00	0.00	0.40	98.7	93.8	56.9
PK14-09 Ol@10	Grain 7 core	13.71	0.78	1.25	0.62	40.9	0.01	0.00	0.01	6.10	0.10	51.1	0.14	0.18	0.06	0.48	99.1	93.8	62.0
PK14-41 Serp@1		-23.14	1.76	0.17	0.25	40.5	0.00	0.04	0.06	3.00	0.04	38.8	0.07	0.01	0.00	0.48	83.0	95.9	82.1
PK14-41 Serp@2		-21.80	1.23	0.24	0.12	40.6	0.00	0.03	0.03	3.28	0.04	37.7	0.04	0.02	0.02	0.37	82.2	95.4	79.0
PK14-41 Serp@3		-8.73	1.50	0.18	0.06	42.3	0.00	0.04	0.03	2.92	0.04	38.8	0.07	0.02	0.02	0.15	84.4	96.0	79.9

PK14-41 Serp@4	-12.08	2.19	0.09	0.03	41.0	0.00	0.08	0.01	2.86	0.03	37.6	0.05	0.00	0.02	0.41	82.0	95.9	90.9
PK14-41 Serp@5	-9.72	2.12	0.11	0.08	41.4	0.01	0.06	0.02	2.77	0.06	37.7	0.09	0.02	0.02	0.29	82.4	96.1	47.1

Note: Ol, olivine; Serp, serpentine; PK14-41 Serp@1 to @5, increasing distance away from chromite nodule.